

REFERENCES AND NOTES

- D. Jablonski, *Science* **231**, 129 (1986); *ibid.* **253**, 754 (1991).
- D. H. Erwin, *The Great Paleozoic Crisis: Life and Death in the Permian* (Columbia Univ. Press, New York, 1993); *Nature* **367**, 231 (1994).
- L. M. Van Valen, in *Mass Extinction Debates*, W. Glen, Ed. (Stanford Univ. Press, Stanford, CA, 1994), pp. 200–216.
- D. Jablonski, *Philos. Trans. R. Soc. London Ser. B* **344**, 11 (1994).
- Updated from D. M. Raup and D. Jablonski, *Science* **260**, 971 (1993). A full bibliography of sources is available from the authors.
- D. Jablonski, *Bull. Mar. Sci.* **39**, 565 (1986).
- G. L. Wingard and N. F. Sohl, *U.S. Geol. Surv. Bull.* **1881**, D1 (1990); G. L. Wingard, *U.S. Geol. Surv. Prof. Pap.* **1535**, 1 (1994).
- K. G. MacLeod and P. D. Ward, *Geol. Soc. Am. Spec. Pap.* **247**, 509 (1990); K. G. MacLeod, *Geology* **22**, 139 (1994); *J. Paleontol.* **68**, 1048 (1994).
- E. G. Kauffman, in *Global Bio-Events*, O. H. Walliser, Ed. (Springer-Verlag, Berlin, 1986), pp. 279–335; C. C. Johnson and E. G. Kauffman, in *Extinction Events in Earth History*, E. G. Kauffman and O. H. Walliser, Eds. (Springer-Verlag, Berlin, 1990), pp. 305–331.
- P. D. Ward, W. J. Kennedy, K. MacLeod, J. Mount, *Geology* **19**, 1181 (1991). Our own data suggest that other bivalves lack any decline parallel to that of the inoceramids, both in the Gulf and Atlantic Coastal Plain [D. Jablonski, in *Dynamics of Extinction*, D. K. Elliot, Ed. (Wiley, New York, 1986), pp. 183–229] and in the classic Denmark sections.
- L. Marincovich Jr., *Paleontol. Soc. Mem.* **35** (*J. Paleontol.* **67**, suppl. to no. 5), 1 (1993).
- E. G. Kauffman, *Philos. Trans. R. Soc. London Ser. B* **284**, 277 (1978).
- S. M. Stanley, *Paleobiology* **12**, 89 (1986).
- Life habits were inferred by analogy with living relatives of similar morphology and were based on widely used criteria available in the functional morphology literature. See S. M. Stanley, in *The Mollusca*, vol. 11, *Form and Function*, E. R. Trueman and M. R. Clarke, Eds. (Academic Press, San Diego, CA, 1988), pp. 105–141.
- R. H. Peters, *The Ecological Implications of Body Size* (Cambridge Univ. Press, Cambridge, 1983); W. A. Calder, *Size, Function, and Life History* (Harvard Univ. Press, Cambridge, MA, 1984).
- S. L. Pimm, H. L. Jones, J. Diamond, *Am. Nat.* **132**, 757 (1988); M. K. McKinney, in *Evolutionary Trends*, K. J. McNamara, Ed. (Univ. of Arizona Press, Tucson, 1990), pp. 75–118; J. H. Brown, P. A. Marquet, M. L. Taper, *Am. Nat.* **142**, 573 (1993); but see R. A. Martin, *Historical Biology* **6**, 73 (1992).
- D. J. Bottjer and D. Jablonski, *Palaio* **3**, 540 (1988).
- J. J. Sepkoski Jr., *Science* **235**, 64 (1987).
- D. H. Erwin, *Palaio* **4**, 424 (1989); see also S. R. Westrop, *Paleobiology* **15**, 46 (1989).
- J. E. Sorauf and A. E. H. Pedder, *Can. J. Earth Sci.* **23**, 1265 (1986).
- G. R. McGhee, in *Mass Extinctions*, S. K. Donovan, Ed. (Columbia Univ. Press, New York, 1989), pp. 133–151.
- We divided the world into the 16 Late Cretaceous provinces recognized by E. G. Kauffman, in *Atlas of Palaeobiogeography*, A. Hallam, Ed. (Elsevier, Amsterdam, 1973), pp. 353–383.
- The maximum difference between extinction intensities occurs when restricted taxa are defined as less than two or three provinces, suggesting a threshold effect. For example, for nonrudist taxa restricted to ≤ 2 provinces, the extinction rate is $64 \pm 7\%$ [see (32)], whereas taxa in ≥ 3 provinces have an extinction rate of $48 \pm 8\%$. If the cutoff is set between three and four provinces, extinction intensities are $62 \pm 7\%$ and $46 \pm 9\%$, respectively. If inoceramids are omitted, the differential between widespread and restricted taxa increases slightly.
- Reviewed by D. Jablonski, in *Extinction Rates*, J. H. Lawton and R. M. May, Eds. (Oxford Univ. Press, Oxford, 1995), pp. 25–44; *Geol. Soc. Am. Spec. Pap.*, in press.
- G. Keller, *Mar. Micropaleontol.* **21**, 1 (1993); _____, E. Barrera, B. Schmitz, E. Mattson, *Geol. Soc. Am. Bull.* **105**, 979 (1993); but see B. T. Huber *et al.* *Mar. Micropaleontol.* **24**, 91 (1994).
- For nonmarine communities, see P. M. Sheehan and T. A. Hansen, *Geology* **14**, 868 (1986); P. M. Sheehan and D. E. Fastovsky, *ibid.* **20**, 556 (1992). For marine communities, see G. R. McGhee (21); M. C. Rhodes and C. W. Thayer, *Geology* **19**, 877 (1991); C. R. C. Paul and S. F. Mitchell, *ibid.* **22**, 679 (1994).
- R. G. Reid and D. G. Brand, *Veliger* **29**, 3 (1986); C. S. Hickman, *ibid.* **37**, 43 (1994); P. R. Dando *et al.*, *Mar. Ecol. Prog. Ser.* **107**, 169 (1994).
- R. Pohlo, *Proc. Malacol. Soc. London* **38**, 361 (1969); J. S. Levinton, *Mar. Biol.* **110**, 375 (1991); P. Kamermans, *Mar. Ecol. Prog. Ser.* **104**, 63 (1994); J. Lin and A. H. Hines, *Oikos* **69**, 28 (1994).
- K. Roy, *Paleobiology* **20**, 274 (1994).
- P. A. Jumars *et al.* [*Philos. Trans. R. Soc. London Ser. A* **331**, 85 (1990)] distinguish among surface deposit-feeders such as the tellinids, subsurface deposit-feeders such as the nuculoids, and chemautotrophic deposit-feeders such as the lucinoideans.
- P. A. Tyler, *Oceanogr. Mar. Biol. Annu. Rev.* **26**, 227 (1988); A. J. Gooday and C. M. Turley, *Philos. Trans. R. Soc. London Ser. A* **331**, 119 (1990); P. J. D. Lambshead and A. J. Gooday, *Deep-Sea Res.* **37**, 1263 (1990); M. A. Rex *et al.*, *Nature* **365**, 636 (1993); L. S. Campos-Creasey *et al.*, *Deep-Sea Res.* **41**, 369 (1994); M. Nakaoka, *Mar. Ecol. Prog. Ser.* **88**, 215 (1992).
- We calculated the 95% confidence limits explicitly by summing binomial probabilities using a program given by D. M. Raup, in *Analytical Paleobiology*, N. L. Gilinsky and P. W. Signor, Eds. (Paleontological Society, Knoxville, TN, 1991), pp. 207–216.
- We thank S. Calzada, R. J. Cleavelly, A. V. Dhondt, C. Heinberg, E. G. Kauffman, G. L. Kennedy, M. Machalski, N. Malchus, L. Marincovich Jr., N. J. Morris, L. R. Saul, J. J. Sepkoski Jr., N. F. Sohl, T. R. Waller, and L. R. Wingard for advice and access to collections or information. We thank D. B. Rowley for the Maastrichtian latitude-longitude conversions for bivalve sample sites and G. E. Boyajian, S. M. Kidwell, J. S. Levinton, A. I. Miller, and J. J. Sepkoski Jr. for discussions and reviews. We are especially grateful to A. Koziol, D. McShea, and J. Schneider for undertaking the initial literature search and data compilation. Supported by NSF grants EAR93-17114 and INT86-2045 (D.J.) and National Aeronautics and Space Administration grants NAGW-1508 and 1527 (D.M.R.). D.J. did much of this work as a research associate of the Natural History Museum, London.

17 November 1994; accepted 27 February 1995

Seismic Images of Active Magma Systems Beneath the East Pacific Rise Between 17°05' and 17°35'S

John C. Mutter, Suzanne M. Carbotte, Wusi Su, Liqing Xu, Peter Buhl, Robert S. Detrick, Graham M. Kent, John A. Orcutt, Alistair J. Harding

Seismic reflection data from the East Pacific Rise between 17°05' and 17°35'S image a magma lens that varies regularly in depth and width as ridge morphology changes, confirming the notion that axial morphology can be used to infer ridge magmatic state. However, at 17°26'S, where the ridge is locally shallow and broad, the magma lens is markedly shallower and wider than predicted from regional trends. In this area, submersible dives reveal recent volcanic eruptions. These observations indicate that it is where the width and depth of the magma chamber differ from regional trends, indicating an enhanced magmatic budget, that is diagnostic of current magmatism.

On fast-spreading ridges, such as the East Pacific Rise (EPR) south of the Garrett fracture zone, axis morphology is characterized by a prominent bathymetric high with smooth flanks and a relatively flat summit about 2 km wide, standing ~400 m above the regional sea floor (1). The depth of the axis and the cross-sectional area of the axial high change along the axis in a sympathetic manner, the shallowest regions generally having the broadest cross sections (2, 3). These "inflated" regions are thought to overlie centers of magma upwelling (1, 2, 4–6), the enlarged shape being an expression of volcanic tumescence. The summit

region of the axial high often includes a small, narrow depression, now commonly referred to as the axial summit caldera (ASC) (7), believed to be the product of magma withdrawal and subsequent collapse. In some inflated regions, the ASC is absent, perhaps because of a recent filling of the depression with lava (8). These variations in axial morphology have been interpreted as reflecting variable magma supply along the ridge axis (2, 5, 6).

Seismic reflection imaging provides another indicator of variable magmatic activity. The horizon marking the top of the axial magma chamber (AMC) is typically observed beneath broad, shallow regions of the ridge and is absent or less commonly observed beneath narrow, deep regions (8, 9). In a few areas of the EPR, near-bottom observations of recent volcanic activity (10) provide further support for the conjecture that a broadened ridge profile, shallow axial

J. C. Mutter, S. M. Carbotte, W. Su, L. Xu, P. Buhl, Lamont-Doherty Earth Observatory of Columbia University, Box 1000, Palisades, NY 10964, USA. R. S. Detrick and G. M. Kent, Woods Hole Oceanographic Institution, Woods Hole, MA 02543, USA. J. A. Orcutt and A. J. Harding, Scripps Institution of Oceanography, La Jolla, CA 92093, USA.

depths, and a shallow AMC reflector can be used as proxies for the state of magmatic activity of the ridge where direct observations are not available. Here we present results of a geophysical study that included a dense array of seismic reflection lines of the ultrafast-spreading southern EPR (150 to 155 mm/year, full rate) from about 17°05' to 17°35'S (Fig. 1) (11). Recent volcanic eruptions have been observed at two locations within this area: at 17°26' and 17°08'S. From seismic images of the AMC and upper crust, we examined the relation of magma distribution in the subsurface and magmatically active areas of the ridge.

At 17°26'S, axial depths are about 50 m less than the regional average, the ridge displays a broad cross section, and the summit lacks evidence of an ASC (1, 3) (Fig. 1). Shoaling and broadening of the axial high occurs over about 15 km along the ridge. An AMC reflector is present, and observations from submersible dives and bottom photographs reveal recent eruptions (12). The enlarged region centered at 17°08'S is not as shallow as the one at 17°26'S but is broader (Fig. 1). An AMC reflector is present here also, and very fresh volcanics are observed (12). Comparison of dive observations and dredging in the area over the past 10 years suggests that although eruption is extremely recent at both locations, eruptions at 17°26'S may have occurred more recently (13). Although dive observations are not available for the intervening ridge segment, older volcanic rocks do appear to crop out away from the center of the inflated region at 17°26'S (12, 14), and we assume that the inflated regions are probably the sites of the most recent volcanism along this ridge segment. There is evidence for eruption in the 17°26'S area just prior to a near-bottom study of the region in 1984, and it is possible that this portion of the ridge has been in a near continuous state of eruption over the past decade (15, 16).

Seismic reflection data were collected along the ridge axis and along a series of lines crossing the ridge (Fig. 1) (17). The along-axis seismic image (Fig. 2A) was obtained by profiling as near as possible to the center of the axial high with the Hydrosweep swath mapping system (18). The most prominent feature in the image is the AMC reflector, which occurs at an average depth of 1200 m beneath the sea floor (Fig. 2A). In the inflated area centered at 17°26'S, the AMC broadly arches upward beneath the shoaling sea floor over an along-axis distance of about 15 km (from ~17°20' to 17°29'S) (Figs. 2A and 3, A and B). Although the sea floor rises by about 50 m (hardly noticeable in Fig. 2A), the AMC horizon shoals by over 200 m. Similar shoaling of the AMC with respect to the sea floor is also observed at the volcanically active EPR at 9°45'N (10, 19).

Because the AMC is on the order of 1 km in width in these areas and assuming that the present configuration is not steady state, the magma body must have risen into a preexisting basalt section. Presumably, if this occurred, a portion of the lower sheeted dike complex was consumed into the magma chamber by stoping, a process that would allow hydrated basalt to enter the magma.

These images and earlier studies of the EPR (9, 11, 19–23), together with observations reported from other areas, suggest that average AMC depth varies inversely with spreading rate (24). The AMC depths in the inflated areas within the 17°05' to 17°35'S region are among the shallowest observed. At 17°25'S, near the crest of the broader regional arch, the AMC locally reaches to within about 800 m of the sea floor (centered near line 1107, Figs. 2A and 3B). This local high is not observed near 17°08'S and has no counterpart elsewhere on the EPR. These characteristics in conjunction with dive observations (12) suggest that we imaged an erupting magma lens at 17°26'S.

The cross-axis lines 1106 to 1114 reveal further the characteristics of the magma system (Fig. 2, B and C). Along these lines we measured the width and depth of the AMC, together with the thickness of seismic layer 2A (Fig. 3). Sea-floor characteristics of axial depth and cross-sectional area (3) were also

examined. The properties measured on cross-axis lines do not always correspond to those seen on line 1115 (Fig. 3) because the along-axis line strays off the center of the ridge. The measured properties at the ridge center point on the cross-axis lines more accurately characterize the zero-age properties of the ridge axis.

The AMC reflector is presumed to mark the liquid melt that provides the source for the dike and extrusive sequences, and its width may be a rough proxy for the ridge's magmatic state. The depth of the AMC may also be a strong local indicator of magmatic state, and swelling of the ridge's cross section could be a precursor to an eruption or an indicator of current activity. The base of seismic layer 2A (the upper crustal low-velocity layer) is imaged in seismic reflection data collected with long receiving arrays. In these data, a strong arrival is observed, which corresponds to diving (turning) rays that turn energy within a steep velocity gradient (from 2.4 to 5 km/s in less than 100 m), which defines the base of this layer. Layer 2A is commonly ~100 to 200 m thick on the axis and approximately doubles in thickness within 1 to 2 km of the axis (19, 22, 23). Seismic layer 2A is believed to correspond to the extrusive basalt section (11) and hence is the eruptive product of the magma system. It is reasonable to suppose

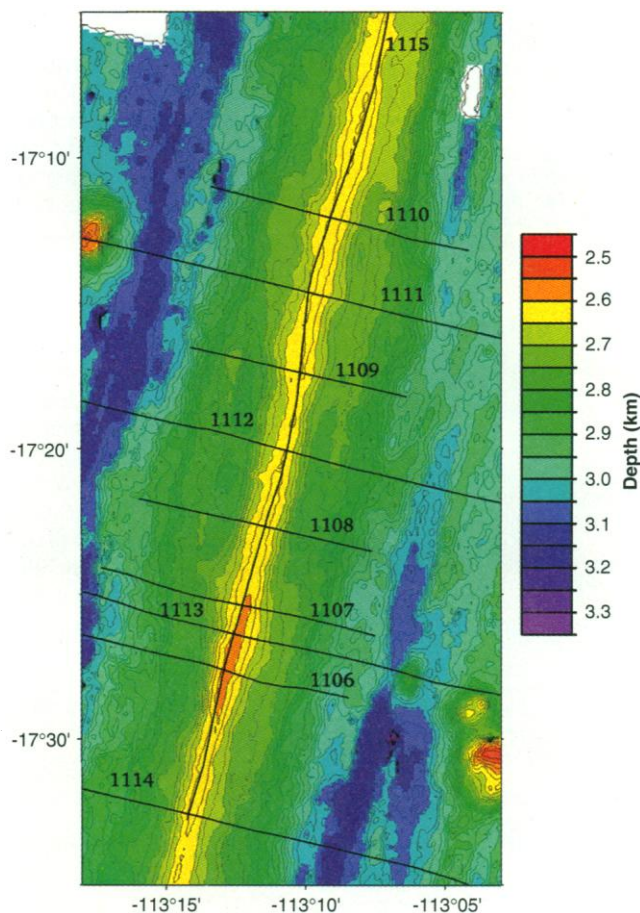


Fig. 1. Surface morphology of a segment of the EPR south of the Garrett fracture zone obtained from Hydrosweep multibeam imaging. Portions of the rise axis centered at 17°26' and 17°08'S are "inflated," being broader and shallower than adjacent regions. The numbered lines refer to ship tracks along which seismic images were obtained (Fig. 2) and from which estimates of properties of the subsurface related to the local magmatic state have been measured (Fig. 3).

then that its local thickness may be an indication of the magmatic state of the ridge; greater thicknesses presumably represent greater magmatic activity.

Away from the inflated area at 17°26'S, AMC width and depth vary systematically as a function of axial depth; as the ridge shallows, the AMC broadens and reaches toward the sea floor (Fig. 3, F and G). Variations in AMC depth as a function of width (Fig. 3H) and the ridge cross-sectional area (Fig. 3J) are also approximately linear and systematic. These relations suggest that the surface morphology of the ridge can be used as a reasonably reliable predictor of subsurface characteristics and magmatic state. These general relations do not hold in the erupting area at 17°26'S, where the AMC is both considerably shallower than would be predicted and much broader (Fig. 3, F through J, lines 6, 7, and 13). Furthermore, AMC width and depth vary inversely for most of the region but appear to vary orthogonally in the erupting area at 17°26'S (Fig. 3H). The thickness of layer 2A is, unexpectedly, considerably less in the inflated area at 17°26'S than it is elsewhere along the ridge, except at ~17°15'S (line 1111), where the cross-sectional area of the ridge reaches a local maximum (Fig. 3, D and E). Thus, it appears that regional relations cannot be linearly projected into areas of current eruption to predict AMC characteristics or volcanic-layer thickness.

Several inferences regarding eruption processes at the ridge can be derived from these relations. Even if the thickness of the

melt lens remains constant throughout the region, an increase in AMC width implies a corresponding increase in the volume of magma available for eruption. Hence, the regular increase in AMC width and decrease in its depth associated with shallowing axial water depth may imply a buildup of magma as a precursor to eruption. At locations where eruption is taking place, magma is being removed, presumably giving rise to a narrower AMC as magma withdrawal progresses and providing a plausible explanation for the orthogonal trend in Fig. 3H.

It is commonly assumed that the rise of magma through the crust is primarily controlled by the buoyancy of the melt relative to that of the surrounding country rock (25). The depth at which the magma chamber resides in the crust may correspond with the level of neutral buoyancy for the melt, where its density is equal to that of the local country rock (25). Hoof and Detrick (26) have pointed out that the AMC depths measured to date are considerably greater than are consistent with neutral buoyancy of magma having a density equivalent to typical lavas erupted onto the sea floor (2700 kg/m³). Either the typical density of magma in the AMC is greater or mechanisms other than neutral buoyancy are controlling AMC depth. In our study area, Hoof and Detrick's observation applies to AMC depths along the noninflated areas of the ridge; in the erupting area, AMC depths are more nearly consistent with the expected neutral buoyancy level. Hoof and Detrick suggested that

a mechanical boundary such as a freezing horizon (27), whose depth is controlled by the ridge's thermal structure, prevents magma from rising to its level of neutral buoyancy. Compelling support for the importance of ridge thermal structure on AMC depth comes from its success in accounting for the observed inverse relation between AMC depth and spreading rate (24). Such a scenario leads to the reasonable conjecture that normal areas of the ridge where regular shoaling of the AMC and sea floor is observed are generally hotter. Furthermore, where the AMC shallows abruptly at 17°25'S, the mechanical barrier may have been breached, and magma has risen toward the expected neutrality level.

Ryan (28) has pointed out that the density of melt plus crystals, rather than the density of melt alone, may control the neutral buoyancy level for the AMC. The AMC may indeed always lie at its correct neutrality depth, and the observed variation in AMC depth may reflect changes in aggregate magma plus crystal density. The AMC depths observed in normal regions of the ridge imply a magma density of about 2800 kg/m³, a value that is consistent with a magma in which about 10% olivine crystals are present in a picritic melt (28). Variation in AMC depth may therefore be a proxy for changes in crystal fraction of magma in the reservoir, which could, in turn, be related to thermal state: The hotter the ridge, the more nearly the material approaches a pure liquid. Eruption might occur when a near-liquid state has been achieved. With this model, the observed inverse relation between AMC depths and spreading rate (24) may reflect a larger crystal fraction in the magma reservoir at slower spreading rates. Indeed, highly porphyritic basalts are commonly dredged from the slow-spreading ridges. Another mechanism that could account for density variation is the changes that accompany fractional crystallization. Starting from a picritic magma with a Fe/(Fe + Mg) mole ratio (Fe#) of around 0.2 and a density of 2750 kg/m³, magma evolves to a Fe# of 0.4 associated with a density minimum of 2700 kg/m³. As fractional crystallization continues and Fe# increases to 0.8, density increases to around 2800 kg/m³. Hence, the normal processes of fractional crystallization of magma lead to density changes that encompass the observed variations in AMC depths. Under such a control, eruption might occur when fractional crystallization has caused magma to evolve to its density minimum.

No clear relation is observed between the thickness of layer 2A and other indicators of ridge magmatic state. Indeed, given the inflated ridge morphology and the shallow, wide AMC reflector in the erupting area at 17°26'S, we might have expected a thicker volcanic layer associat-

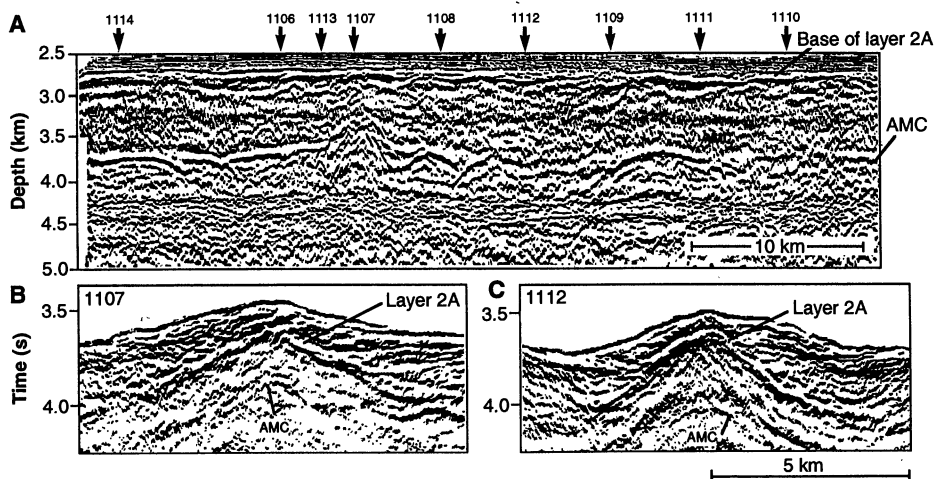


Fig. 2. (A) Seismic image of line 1115 obtained by profiling along the center of the rise axis (Fig. 1). The position of intersection of the cross lines is indicated with arrows. The reflection from the AMC beneath the inflated area at 17°26'S arches upward and includes a distinct peak just north of the cross-axis line 1107, which reaches to within 800 m of the sea floor. The quality of the AMC reflector in this region is poorer than elsewhere along this line presumably because of the locally three-dimensional nature of the reflector. (B) Example of one of the cross lines from the southern inflated area. (C) Example from the region between inflated areas. Wave equation datuming and migration have been carried out on cross-axis lines (17). The final processed images are converted to depth by making a variable stretch to the vertical (time) axis. The velocity function for depth conversion was derived from the stacking velocity analysis and the results of seismic refraction experiments carried out in the same area (17).

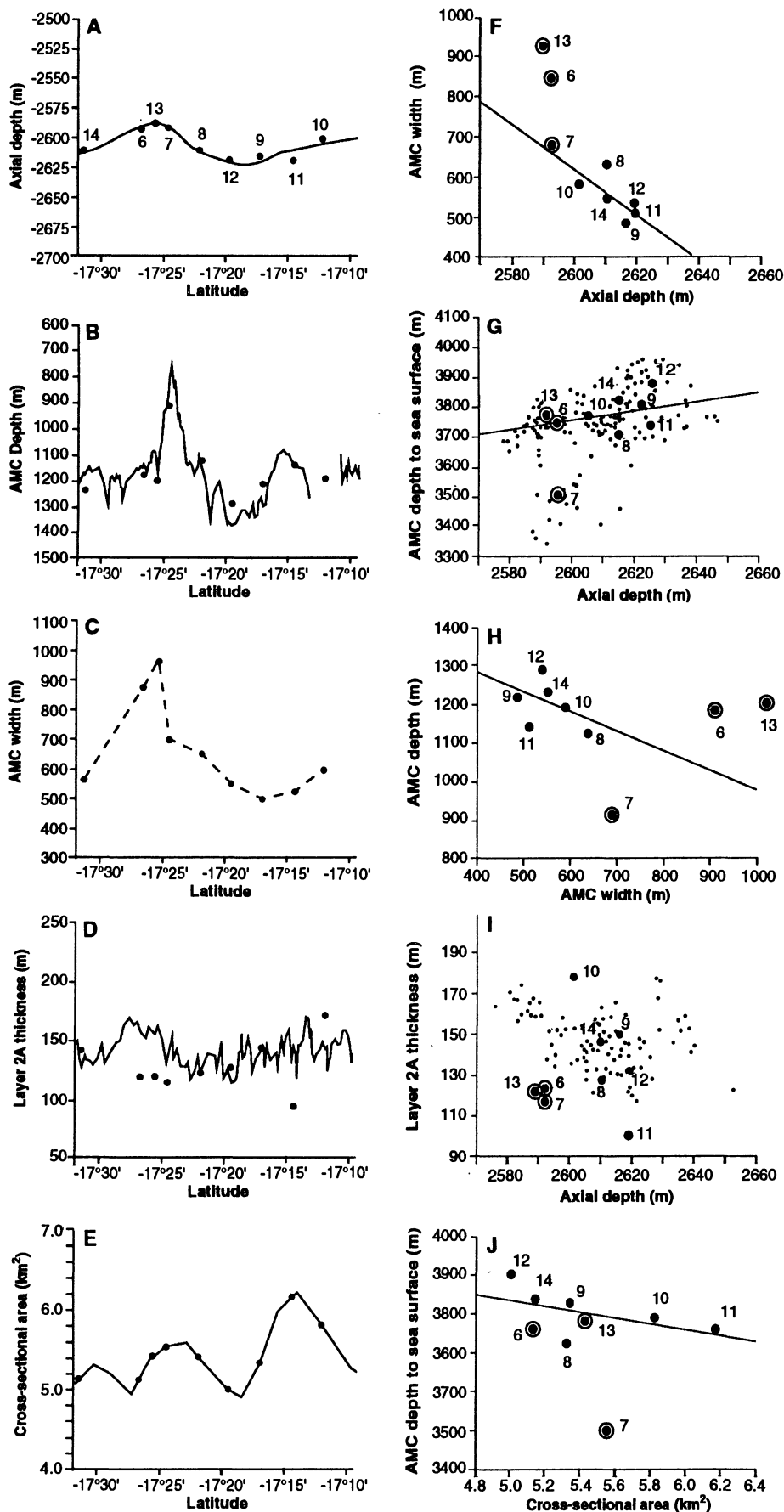


Fig. 3. Properties of the ridge axis that may be used as proxies for magmatic state have been measured from the cross-axis lines (large dots) and the along-axis line (solid line in A to E; small dots in G and I) and are portrayed in two ways: (A through E) in their correct along-axis position and (F through J) so that their variation with axial depth can be seen together with interrelations among axial properties. Measurements of AMC width are available only from cross lines. Cross-sectional area estimates are from (3). Data away from the erupting area at 17°26'S show fairly regular variations with axial depth and cross-sectional area, suggesting that surface morphology is a fairly reliable indicator of magma chamber characteristics. Data from the erupting area at 17°26'S (circled points 1106, 1107, and 1113) fall off these approximately regular trends, and it is these deviations that may be diagnostic of active eruption.

ed with the presumed robust magmatic budget. However, along all cross lines through this area, layer 2A is not only thinner than the average zero-age thickness, it is also markedly thinner (25 to 40 m) than observed immediately outside of the innermost axial zone (Fig. 3D). The lack of a clear relation between layer 2A thickness and the other ridge parameters may reflect the difference in time scale for the magma chamber versus that which governs construction of the volcanic layer. Layer 2A thickness represents the volcanic budget integrated over several thousand years, whereas the other parameters measured describe the present, almost instantaneous magmatic state. Growth rates for the volcanic layer are not well known, but they presumably cannot on average exceed that required to form the neovolcanic zone (1000 to 3000 years). The thin layer 2A in the erupting areas may reflect a young volcanic layer that has not yet attained its full thickness, whereas it is more fully developed in the intervening regions. This interpretation is consistent with the notion that we have imaged the creation of an element of oceanic crust at 17°26'S.

REFERENCES AND NOTES

1. P. Lonsdale, *J. Geophys. Res.* **94**, 12197 (1989).
2. K. C. Macdonald, J.-C. Sempere, P. J. Fox, *ibid.* **89**, 6049 (1984).
3. D. S. Scheirer and K. C. Macdonald, *ibid.* **98**, 7871 (1993).
4. J. A. Whitehead Jr., H. J. B. Dick, H. Schouten, *Nature* **312**, 146 (1984).
5. C. H. Langmuir, J. F. Bender, R. Batiza, *ibid.* **322**, 422 (1986).
6. D. W. Forsyth, in *Mantle Flow and Melt Generation at Mid-Ocean Ridges*, J. Phipps Morgan, D. K. Blackman, J. M. Sinton, Eds. (*Geophys. Monogr.* **71**, American Geophysical Union, Washington, DC, 1992), pp. 1-65.
7. R. M. Haymon *et al.*, *Earth Planet. Sci. Lett.* **104**, 513 (1991).
8. K. C. Macdonald and P. J. Fox, *ibid.* **88**, 119 (1988).
9. R. S. Detrick *et al.*, *Nature* **326**, 35 (1987).
10. R. M. Haymon *et al.*, *Earth and Planet. Sci. Lett.* **119**, 85 (1993).

11. R. S. Detrick *et al.*, *Science* **259**, 499 (1993).
12. J.-M. Auzende *et al.*, *Eos* **75**, 601 (1994).
13. J. M. Sinton *et al.*, *ibid.* (fall suppl.), p. 320.
14. M.-H. Cormier, personal communication.
15. V. Renard *et al.*, *Earth Planet. Sci. Lett.* **75**, 339 (1984).
16. K. C. Macdonald, D. S. Scheirer, S. Carbotte, P. J. Fox, *GSA Today* **3**, 1 (1993).
17. Seismic data were collected from Lamont-Doherty's research vessel *R/V Maurice Ewing* by a 20-element air-gun source array, with a total volume of 8400 cubic inches, and a 4-km-long, 160-channel Digicon (Houston, TX) digital streamer. Routine processing was carried out on a CONVEX 3420 mini-supercomputer at Lamont-Doherty running Western Geophysical's Omega seismic processing package. The processing sequence was specifically designed to take account of the detrimental effect of the rough sea-floor topography on the image of the AMC. Stacking velocity analyses were performed at a particularly dense spatial increment of 100 to 200 m. Stacked images were then processed with a wave equation datuming procedure recently developed by W. Su and J. C. Mutter (in preparation) that reduces the observations to the sea floor by carrying out wave-field extrapolation in the Radon domain. This procedure uses information on the shape of the sea floor derived from the Hydrosweep swath mapping system (18) installed on the *Ewing* and largely compensates for ray bending across the sea-floor interface that distorts the image of structure beneath. These images can then be used to estimate the width and shape of the AMC.
18. D. N. Chayes, *IEEE* **2**, 737 (1991).
19. E. Vera and J. B. Diebold, *J. Geophys. Res.* **99**, 3031 (1994).
20. E. Vera *et al.*, *ibid.* **95**, 15529 (1990).
21. A. J. Harding *et al.*, *ibid.* **94**, 12163 (1989).
22. G. M. Kent *et al.*, *ibid.* **99**, 9097 (1994).
23. A. J. Harding, G. M. Kent, J. A. Orcutt, *ibid.* **98**, 13925 (1993).
24. G. M. Purdy, L. S. L. Kong, G. L. Christensen, S. C. Solomon, *Nature* **355**, 815 (1992).
25. M. P. Ryan, in "Magmatic Processes: Physicochemical Principles," B. O. Mysen, Ed., *Spec. Publ. Geochem. Soc. No. 1* (1987), p. 259.
26. E. E. Hooft and R. S. Detrick, *Geophys. Res. Lett.* **20**, 423 (1993).
27. J. Phipps Morgan and Y. J. Chen, *J. Geophys. Res.* **98**, 6283 (1993).
28. M. P. Ryan, *ibid.*, p. 22321.
29. We thank two anonymous reviewers for their careful reviews. We thank the officers, crew, and staff of the *R/V Maurice Ewing* and *R/V Thomas Washington*. We thank J. Alsop for her aid with data processing and Western Geophysical for provision of software. This work was supported by NSF grants OCE90-12781 and OCE94-03605 to J.C.M. Lamont-Doherty Earth Observatory contribution 5317.

14 October 1994; accepted 17 January 1995

The Collapse of Free Polymer Chains in a Network

Robert M. Briber,* Xiaodu Liu, Barry J. Bauer

The conformation of linear polymer chains trapped in a matrix of cross-linked polymer has been measured by neutron scattering. Three regimes were found depending on the length of the linear chain, N_ℓ , with respect to the mesh size of the network, N_c . When $N_c > N_\ell$, the radius of gyration, R_g , of the linear chain is the same as that observed in the uncross-linked melt. When $N_c < N_\ell$, R_g shrinks according to the scaling relation $R_g^{-1} \sim N_c^{-1}$ that has been predicted for isolated polymer chains trapped in a field of random obstacles. When $N_c \ll N_\ell$, the linear chains are observed to segregate.

The conformation of linear polymer chains trapped in a network is an important problem having relevance in many fields ranging from transport through membranes, polymers in microporous structures, diffusion, and gel electrophoresis (1–9). Polymer networks are one type of constrained environment, and the conformational behavior of dilute, isolated polymer chains trapped in a network should provide important insight into the behavior of polymers in other settings. Indeed, the early treatment of reptation to describe the diffusion of polymers was developed specifically for the case of a linear chain diffusing through a tightly cross-linked melt (1); these results should be compared to recent results showing that the diffusion of long linear chains in a network becomes

slower than expected for a melt (5). If the conformation of the diffusing chain depends on the network density, then the dynamics of the polymer may be affected. Earlier attempts to measure the conformation of linear chains trapped in a network have been hampered by phase separation of the chains (10) and by the fact that only a limited range of concentrations and cross-link densities were examined (11). These past studies have found that the linear chains have the same conformation in a network as in the melt for the systems that remained single-phase.

The question of the conformation of a linear chain trapped in a network resembles the problem of the conformation of a polymer chain in a field of randomly placed obstacles with the cross-link points acting as the obstacles. The conformation of a polymer chain in a field of obstacles has been the subject of considerable recent theoretical work and computer simulations (12–19). In general, it has been found that the radius of gyration of the chain, R_g , depends on the

obstacle density. Muthukumar and others (12–18) have found that when the density of obstacles is small, there is a transition from self-avoiding walk statistics for the polymer chain (that is, excluded volume statistics) to Gaussian behavior. When the density of the obstacles is higher, a transition from the Gaussian state to a localized collapsed state occurs. Gersappe *et al.* (19) have argued for a somewhat different picture in which the chain statistics remain unaltered by the presence of the obstacles and the changes in R_g with increasing obstacle density operate only through the prefactor for R_g .

The calculation by Edwards and Muthukumar (16) showed that, when the obstacle density is sufficiently high and the polymer chain has started to shrink from its unperturbed dimensions, R_g scales with the density of the obstacles (ρ) as

$$R_g^2 \sim \frac{1}{\rho^2} \quad (1)$$

If the obstacles correspond to the cross-link points of the polymer network, then the number of obstacles will scale inversely with the mesh size of the network, N_c (20)

$$\rho \sim \frac{1}{N_c} \quad (2)$$

Therefore, R_g of the linear chains should scale with N_c , as (21)

$$R_g^{-1} \sim N_c^{-1} \quad (3)$$

This report will describe small-angle neutron scattering (SANS) experiments to measure the scattering from linear chains trapped in a network extrapolated to the limit of infinite dilution of the linear chains. We attempt to assess whether the conformation of a linear chain trapped in a network can be described by the scaling behavior derived from the studies of polymer chain conformation in a field of random obstacles.

To make samples of linear chains in a network that could be studied by neutron scattering, we dissolved a narrow molecular weight distribution of anionically polymerized deuterated linear polystyrene with a weight-average molecular weight, $M_w = 79,200$ (linear chain length, $N_\ell = 760$) and $M_w/M_n = 1.05$ (M_n is the number-average molecular weight) in styrene monomer than contained a small amount of divinylbenzene as the cross-linking agent. Free radical polymerization was used to form the polystyrene network around the linear chains. Earlier experiments have shown that this method of synthesizing networks containing linear chains does not result in significant grafting of the polymerizing network to the linear chains (22). It probably would not have been possible to prepare the samples for these experiments by diffusing the linear chains into the network from the outside because of kinetic constraints, espe-

R. M. Briber and X. Liu, Department of Materials and Nuclear Engineering, University of Maryland, College Park, MD 20742, USA.

B. J. Bauer, Polymers Division, National Institute of Standards and Technology, Gaithersburg, MD 20899, USA.

*To whom correspondence should be addressed.